Transactions of the Indian National Academy of Engineering (2022) 7:549–564
https://doi.org/10.1007/s41403-021-00279-y

ORIGINAL ARTICLE

The Multiaxial Creep–Fatigue Failure Mechanism of Mod. 9Cr-1Mo Steel Under Non-proportional Loading: Effect of Strain Energy on Failure Lives

Fumio Ogawa[1] · Yuta Nakayama[2] · Noritake Hiyoshi[3] · Ryuta Hashidate[4] · Takashi Wakai[4] · Takamoto Itoh[5]

Received: 29 July 2021 / Accepted: 2 October 2021 / Published online: 11 October 2021

Abstract
The strain energy-based life evaluation method of Mod. 9Cr-1Mo steel under non-proportional multiaxial creep–fatigue loading is proposed. Inelastic strain energy densities have been calculated as the areas inside the hysteresis loops. The effect of the mean stress has been experimentally considered, and the relationship between inelastic strain energy densities and creep–fatigue lives was investigated. The investigation of hysteresis loops shows that the decrease in the maximum stress leads to a prolonged failure life while stress relaxation during strain holding causes strength reduction. The correction method of inelastic strain energy density has been proposed considering the effect of maximum stress in hysteresis loop and minimum stress during strain holding. Then, strain energy densities for uniaxial and non-proportional multiaxial loading were obtained. Failure life correlation has been performed by calculating theoretical failure life using the relationship between strain energy densities and failure life under uniaxial loading (database). Failure life could be correlated between a factor of 5 (unsafe side) and a factor of 2 (conservation side) band for the proportional loading. Even in the case of non-proportional loading, failure life has been evaluated between a factor of 5 band (unsafe side) and a factor of 3 (conservation side) band. However, failure life of test with strain holding on the tension side with the most prolonged duration (in proportional loading), and test with the lowest strain rate (in non-proportional loading) have been evaluated excessively on the conservation side. This reason is investigated by overlooking hysteresis data, and the mechanisms governing creep-fatigue lives under non-proportional multiaxial loading have been discussed.

Keywords Mod. 9Cr-1Mo steel · Creep–fatigue · Multiaxial loading · Non-proportional loading · Strain energy · Energy-based life evaluation

Introduction

Recently, the improvement of the efficiency of thermal power plants and fast breeder reactors (FBR) is expected, and the condition for their usage is becoming increasingly severe. Therefore, the high-temperature properties of structural material become more critical (Fleischer 1985; Berto et al. 2014; Brnic et al. 2015). Boiler pipes in thermal power plants and vessels for FBR are subjected to creep–fatigue loading due to ordinary usage associated with power on and off at high temperatures (Plumbridge et al. 1982; Doong et al. 1990; Doong and Socie 1991; Wang and Brown 1993). Mod. 9Cr-1Mo steel has superior high-temperature properties with the stability of mechanical properties. As a result, Mod. 9Cr-1Mo steel has been used in thermal power plants and FBR, and the creep–fatigue properties need to be elucidated. Moreover, a life evaluation method needs to be

✉ Fumio Ogawa
fumio.ogawa.d8@tohoku.ac.jp

1 Fracture and Reliability Research Institute, Tohoku University, 6-6-11 Aza-Aoba Aramaki, Sendai-shi, Miyagi 980-8579, Japan

2 Graduate School of Science and Engineering, Ritsumeikan University, 1-1-1 Nojihigashi, Kusatsu-shi, Shiga 525-8577, Japan

3 Division of Engineering, Faculty of Engineering, University of Fukui, 3-9-1, Bunkyo, Fukui-shi, Fukui 910-8507, Japan

4 Japan Atomic Energy Agency, 4002 Narita-cho, O-arai, Ibaraki 311-1393, Japan

5 Department of Mechanical Engineering, College of Science and Engineering, Ritsumeikan University, 1-1-1, Noji-higashi, Kusatsu-shi, Shiga 525-8577, Japan

established for the more effective design of components. In the authors' previous study, creep–fatigue tests of the steel at 823 K were performed using uniaxial (push–pull) tests with different strain rates and tests with strain holding (Nakayama et al. 2021). Non-proportional multiaxial tests were also performed using a circle waveform in which the principal direction of strain rotates with time. Specificity was found in the creep–fatigue lives; failure life gets shorter at maximum strain rates, and longer when strain holding was inserted. The life evaluation method was proposed considering the interaction of fatigue and creep using the IS method proposed by Itoh et al., which considers hardening due to non-proportionality (Itoh et al. 2015; Kasamuta et al. 2019) and modified ductility exhaustion rule proposed by Takahashi et al. (Takahashi and Yaguchi 2005). The authors achieved the evaluation of creep–fatigue lives within 1.5 bands, so the results should be helpful for the design of components. However, uncertainty remains in life evaluation due to the weakness of the ductility exhaustion rule in prediction accuracy because it is an empirical rule (Holdsworth 2019). Moreover, the failure mechanism has not been fully understood.

Strain energy has been widely used for the life evaluation of fatigued components (Ozaltun et al. 2011; Scott-Emuakpor et al. 2010). It can be used for life evaluation for various conditions and is the basis for the practical design of structural members. If the creep–fatigue lives can be correlated with strain energies, it should be directly effective for the creation of elements related to standards for nuclear plants and FBR. Some studies adopted strain energy to creep-fatigue loading and succeeded (Payten et al. 2010; Zhu et al. 2012; Mroziński et al. 2021). Theoretical modeling of strain energy and fitting to the experimental data are also reported (Fan et al. 2015; Wang et al. 2016; Huffman 2016). In this study, strain energies of Mod. 9Cr-1Mo under non-proportional multiaxial creep–fatigue loadings at high temperature have been calculated from the experimental hysteresis loops, and life evaluation has been conducted. To the authors' knowledge, estimation of strain energy under non-proportional multiaxial creep–fatigue loading for Mod. 9Cr-1Mo steel has not been performed in the literature. Life evaluation has been performed considering the interaction of creep and fatigue loading. From the results, mechanisms governing the strength reduction under creep–fatigue loading at high temperatures have been discussed.

Experimental Procedure

Material and Specimen

In this study, Mod.9Cr-1Mo steel, a high chromium ferritic steel, was used. Figure 1 shows the geometry and dimensions of a hollow cylindrical specimen with an outer diameter of

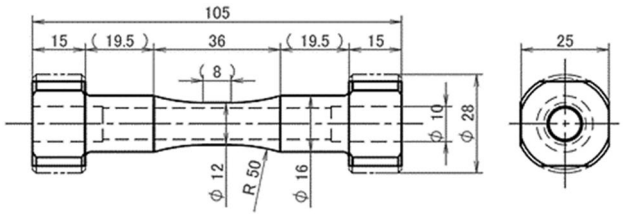

Fig. 1 Shape and dimensions of the specimen (mm)

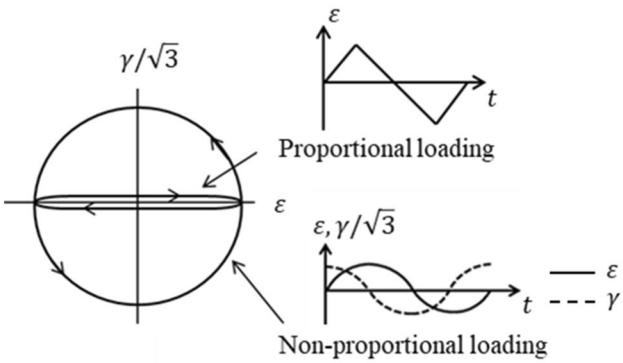

Fig. 2 Strain paths employed in this study

12 mm, an inner diameter of 9 mm, and a parallel section length of 8 mm. The inner and outer surfaces of the specimens were polished with emery paper up to 2000 grit and then buffed with alumina particles up to 1 μm in diameter before testing.

Testing Machine

Two types of electro-hydraulic servo fatigue testing machines are used in this study: one is computer-controlled and can apply axial loading to the specimen, and the other can apply both axial loading and torsional torque. Axial and shear strains are measured using an extensometer equipped with two eddy current displacement sensors. A high-frequency induction heating system was used to heat the test specimens. The temperature of the gauge section was controlled at 823 K by mounting a thermocouple 4 mm below the gauge section. The failure life was defined as the number of cycles when the axial stress amplitude decreased to 3/4 of the change from the steady-state or when specimen fracture was observed.

Strain Waveforms

The two loading modes are employed: push–pull loading (PP) and circle loading (CI), as shown in Fig. 2. PP test is a proportional strain loading test, while the CI test is a non-proportional strain loading test with a 90° phase difference

between axial strain (ε) and shear strain (γ). Figure 3 shows a schematic of the strain waveforms for proportional and non-proportional loading; in the PP test, triangular waveforms with different strain rates were used, and the strain holding was adopted on the tensile or compressive side.

The strain rates for the non-strain-holding tests were 0.2%/s, 0.01%/s and 0.002%/s. In this paper, these are denoted as PP-FF, PP-SS, and PP-SS*, respectively. The strain holding times for the creep-fatigue tests were 3, 10, and 30 min. The strain holding durations for the tensile tests are denoted PP-TH (3 min), PP-TH (10 min), and PP-TH (30 min), and the waveforms with strain holding durations for the compression tests are denoted PP-CH (3 min), PP-CH (10 min) and PP-CH (30 min). The strain rate in the tests with strain holding was 0.2%/s, as in the PP-FF. In the CI tests, sine and cosine waves with different strain rates were used, with the strain holding of the axial strain in tension or compression. The Mises equivalent strain rates for tests without strain holding were 0.2%/s and 0.01%/s. In this paper, these are denoted as CI-FF and CI-SS, respectively. The axial strain holding durations for the creep-fatigue tests were 3, 10, and 30 min in tension, and 3 and 10 min in compression. In this paper, the holding durations on the tensile side are denoted as CI-TH (3 min), CI-TH (10 min), and CI-TH (30 min), and the holding durations on the compressive side are denoted as CI-CH (3 min) and CI-CH (10 min), respectively. The Mises equivalent strain rate for the tests with axial strain holding was 0.2%/s. The Mises equivalent strain range for all tests, both PP and CI tests, was 0.7%.

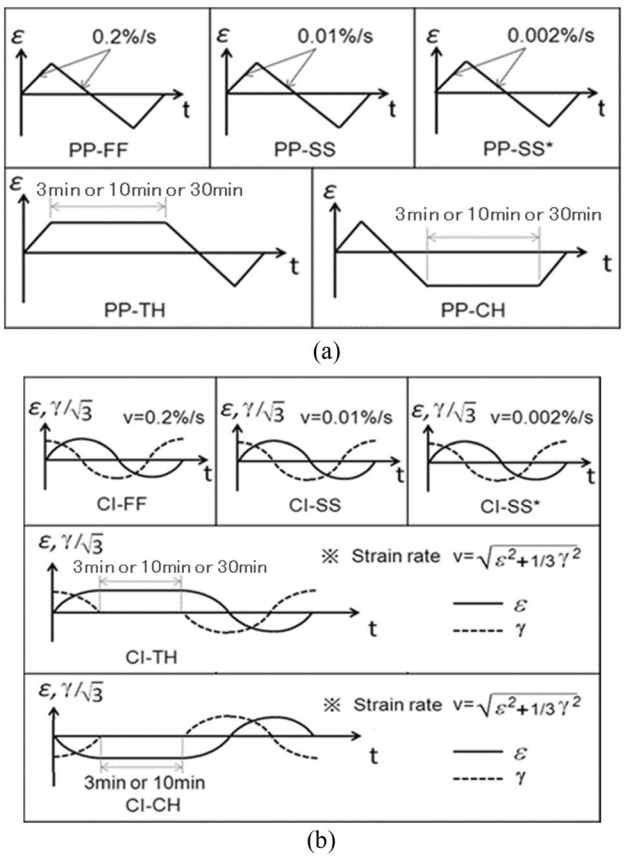

Fig. 3 Strain paths employed in this study: **a** proportional loading, **b** non-proportional loading

Characteristic of Creep–Fatigue Lives

Creep–Fatigue Lives

In this section, creep–fatigue lives have been summarized as the basis for calculating strain energies. Table 1 summarizes failure lives for each test.

In the PP-FF test, of which the strain rate is the highest, failure life is smaller than PP-SS, of which the strain rate is middle. In PP-SS* with the slowest strain rate, failure life gets shorter again. There is a specificity in the dependence on strain rates. Additionally, in PP-TH (3 min), in which strain holding is inserted, failure life is longer than that of PP-FF, owing to the decrease in stress in the tension side as explained later. In PP-CH loadings, failure lives are shorter than PP-TH loading, which will be explained later. In non-proportional loading, similar trends have been observed, although the detail is not ideally the same. That of PP-FF loading has normalized the failure lives, and the trends are shown in Fig. 4. The failure life of PP-SS is about 1.4 times larger than that of PP-FF.

The failure life of PP-SS* nearly equals that of PP-FF. The failure life of PP-TH (3 min) is 1.7 times larger than that of PP-FF. Failure lives of PP-TH (10 min) and PP-TH (30 min) get smaller compared to PP-TH (3 min). This is probably owing to time-effect, i.e., reduction in strength during stress relaxation. In PP-CH (10 min) and PP-CH (30 min), failure lives are smaller than 0.6 times that in PP-FF. In CI-FF and CI-SS loading, failure lives are smaller than 0.6 times that of PP-FF, which is due to the non-proportionality of loading, i.e., stress increment owing to the interaction of dislocations. Failure lives in CI-TH (3 min), and CI-TH (10 min) have been more extensive than CI-FF loading. Failure life in CI-TH (30 min) gets smaller again due to strength reduction during strain holding. Failure lives in CI-CH (3 min) and CI-CH (10 min) are smaller than half of PP-FF, probably because of increased maximum stress due to strain holding on the compression side, as explained later.

Hysteresis Loops Under Proportional Loading

Figure 5 compares the hysteresis loops of PP-FF, PP-SS, and PP-SS* at 1/2 N_f. The maximum stress is the highest among all waveforms for the most enormous strain rate

Table 1 Creep–fatigue lives of Mod. 9Cr-1Mo steel under proportional and non-proportional loading

Loading type	Strain path	Equivalent strain range Δ_{eq} (%)	Waveform	Strain rate (%/s)	Holding period (min)	Failure life N_f (cycles)
Uniaxial/Proportional	Push–pull (PP)	0.7	PP-FF	0.2	–	1150
			PP-SS	0.01	–	1670
			PP-SS*	0.002	–	1133
			PP-TH	0.2	3	1973
				0.2	10	1233
				0.2	30	1114
			PP-CH	0.2	3	1130
				0.2	10	685
				0.2	30	670
Multiaxial/Non-proportional	Circle (CI)	0.7	CI-FF	0.2	–	635
			CI-SS	0.01	–	600
			CI-TH	0.2	3	747
					10	924
					30	780
			CI-CH	0.2	3	510
					10	491

(PP-FF), leading to a smaller failure life. For the lower strain rate, maximum stress gets smaller due to stress relaxation during loading. Failure life gets short because of time-dependent strength reduction during loading.

Figure 6 compares hysteresis loops of PP-FF, PP-TH (3 min), PP-TH (10 min), and PP-TH (30 min) at 1/2 N_f. In PP-TH (3 min), maximum stress is almost the same as PP-FF. However, stress values on the tension side for nearly all strains are smaller than those of PP-FF. Additionally, stress relaxation occurs during tension holding. In PP-TH (3 min), the mean stress value is on the compression side and gets smaller than PP-FF. In PP-TH (10 min) and PP-TH (30 min), maximum stress gets smaller; however, the amount of stress relaxation has been more significant than PP-TH (3 min), which leads to smaller failure life. Absolute values of minimum stresses become smaller than PP-TH (3 min), probably due to the stress relaxation effect.

For the strain holding on the compression side, the maximum stress, consequently the mean stress, can increase compared to PP-FF (Fig. 7). In PP-CH (3 min) and PP-CH (10 min). We find that the maximum stress increases by about 35 MPa, which increases the mean stress. Additionally, stress relaxation occurs on the compression side. For longer holding duration (PP-CH (30 min)), a decrease in maximum stress occurs, in the same way as absolute values of minimum stresses; therefore, the mean stress barely increases. A large amount of stress relaxation takes place, and it decreases failure life. It is estimated that a balance between reduction in life due to relaxation and prolonged life due to the decrease in maximum stress governs failure life.

Hysteresis Loops Under Non-proportional Loading

In the following, we discuss hysteresis loops under non-proportional multiaxial loading. Figure 8 shows hysteresis loops under CI-FF loading. It is clear by comparing with Fig. 5, the data for proportional loading, stress increment under non-proportional loading due to the interaction of dislocations takes place, which decreases failure life in non-proportional loading (Fig. 8a and b) indicates the relation between shear stress and shear strain. In the figure, $1/\sqrt{3}$ times of shear strain range equals 0.7%.

Figure 9 shows the comparison of hysteresis loops of CI-TH (3 min), CI-TH (10 min), and CI-TH (30 min) at 1/2 N_f. Both maximum stress and the absolute value of minimum stress increase in CI-TH (10 min) compared to CI-TH (3 min) (Fig. 9 (a)). In CI-TH (30 min), maximum stress decreases while minimum stress increases, resulting from stress relaxation. Similar trends can be seen in the relationship between shear stress and shear strain. Figure 10 shows the hysteresis loops for the strain holding on the compression side at 1/2 N_f. Axial maximum stress decreases in CI-CH (10 min), while minimum stress decreases, which is the result of the balance between stress relaxation in the compression side and an increase in mean stress (In Fig. 10 (a)). In the relationship between shear stress and shear strain, a decrease in minimum stress occurs in CI-CH (10 min) (Fig. 10 (b)). Simultaneously, an increase in the shear inelastic strain range occurred, reducing failure life.

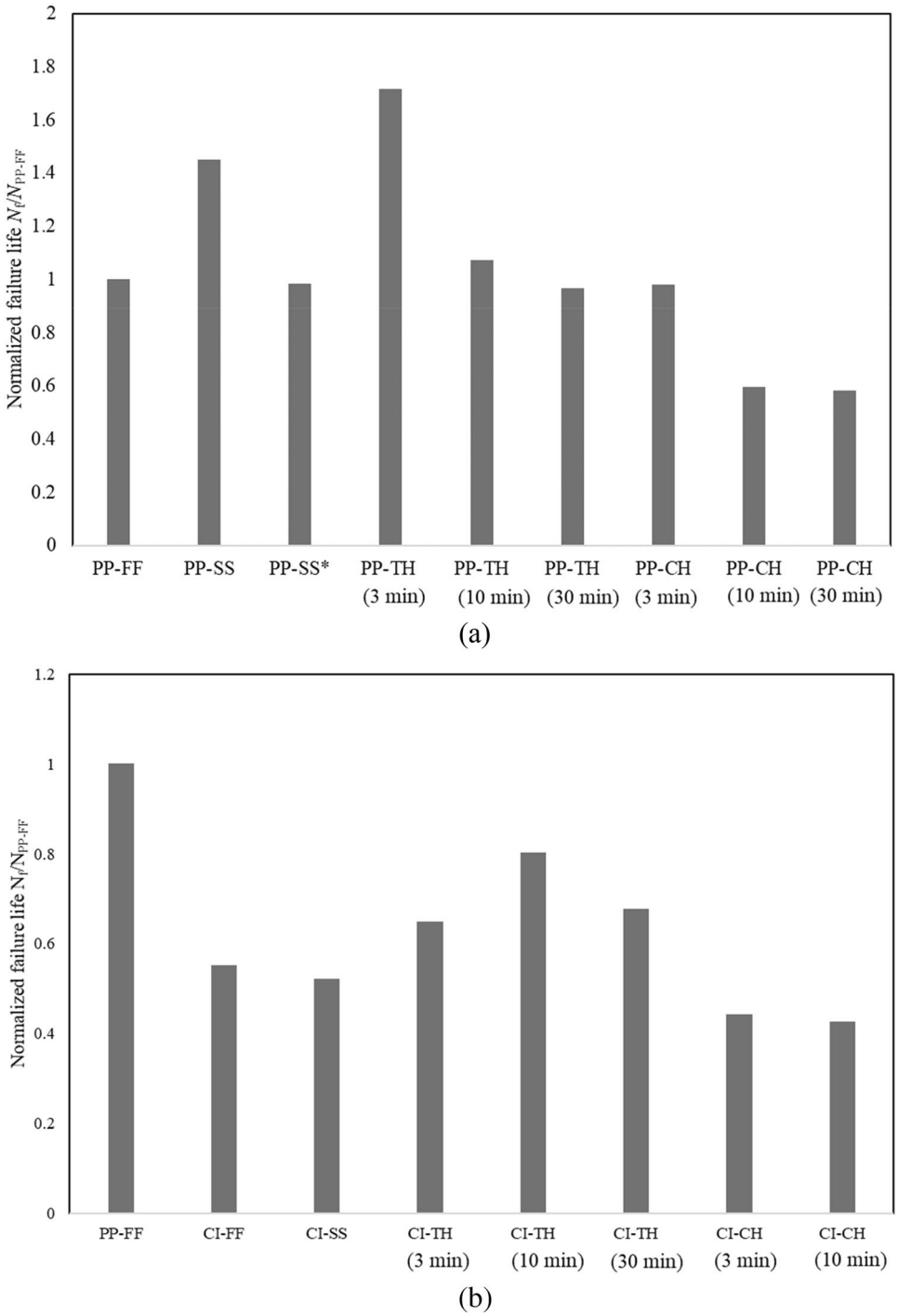

Fig. 4 The normalized creep–fatigue failure lives. **a** Tests based on push–pull loading **b** tests based on multiaxial non-proportional loading

Stress Amplitude and Mean Stress Evolution

This section presents the evolution of stress amplitudes depending on cycles and resultant mean stress variation. Figure 11 (a) shows the stress amplitude under PP-TH (3 min) as a function of creep–fatigue cycles, while Fig. 11 (b) shows the mean stress evolution. Figure 11 (a) demonstrates the maximum and minimum stress for each cycle. Stress amplitude stabilizes just at half of the failure cycle; the plateau of the stress amplitude corresponds to half a failure life. The mean stress decreases with the cycles; it is a characteristic of loading with tension strain holding. The mean stress also stabilizes at half of failure life. Figure 12 (a) shows the stress amplitudes under PP-TH (10 min). Additionally, Fig. 12 (b) shows the mean stress evolution. The stress amplitude stabilizes just at half of failure life. The mean stress does not vary largely from PP-TH (3 min), probably because of the balance between hardening and stress relaxation.

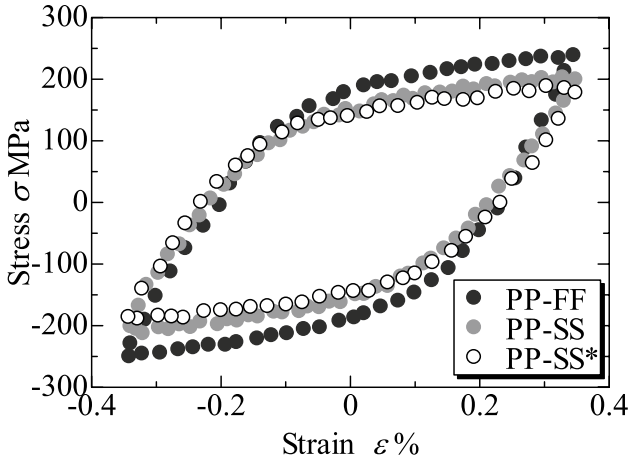

Fig. 5 Hysteresis loops under the push–pull loading

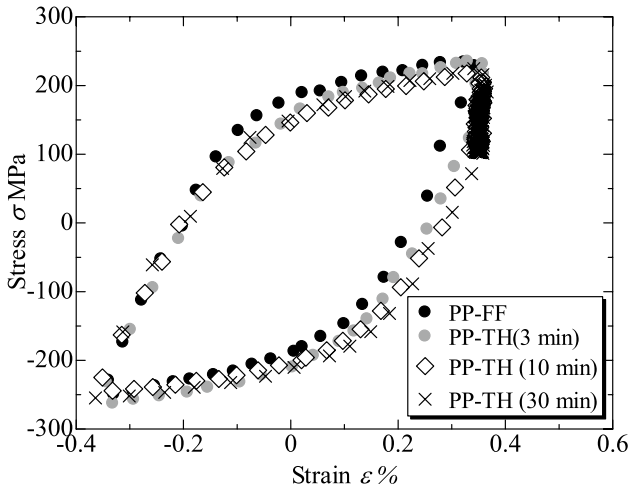

Fig. 6 Hysteresis loops under the PP-TH loading

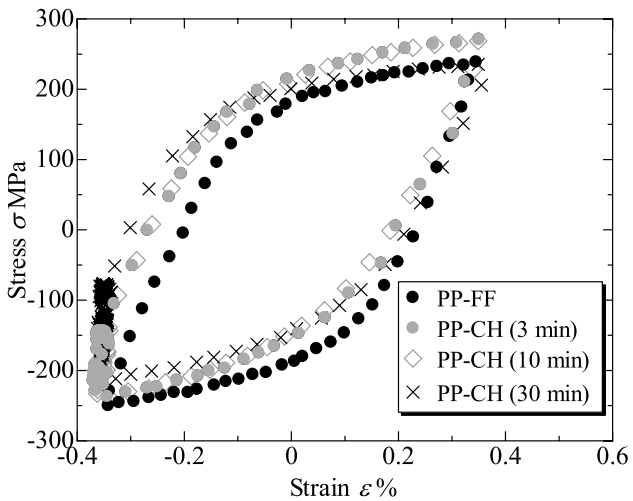

Fig. 7 Hysteresis loops under the PP-CH loading

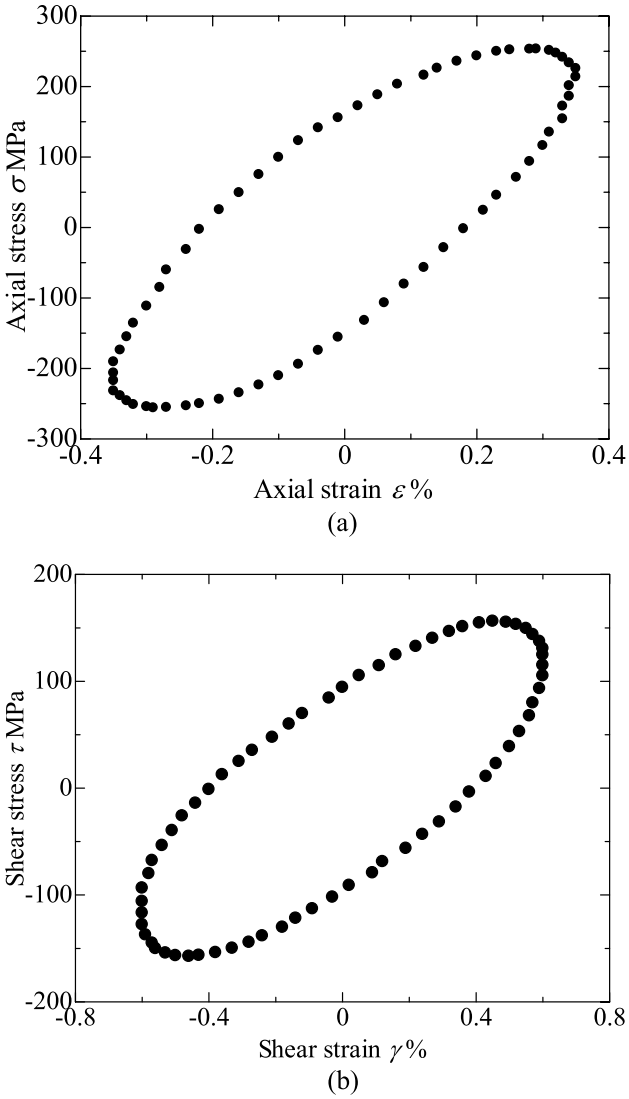

Fig. 8 Hysteresis loops under the CI-FF loading. **a** Axial stress-axial strain **b** shear stress-shear strain

Figure 13 (a) and (b) show the stress amplitude under CI-TH (3 min) loading; Fig. 13 (a) corresponds to the axial stress, while Fig. 13 (b) corresponds to the torsional stress. Stress amplitude stabilizes just at half of failure life. It justifies the calculation of strain energy at half of failure life, as mentioned later. Figure 13 (c) shows the variation of mean axial stress with cycles. The stress varies from negative to positive value due to tension strain and torsional strain. Figure 13 (d) shows the variation of torsional stress, which indicates that torsional stress is dominant under tension strain holding, and the stabilization of stress takes place at half of failure life. Figure 14 (a) shows the axial stress amplitude under CI-CH (3 min), while Fig. 14 (b) shows the torsional stress amplitude. It is clear again that stress amplitudes stabilize just at half of failure life. Figure 14 (c)

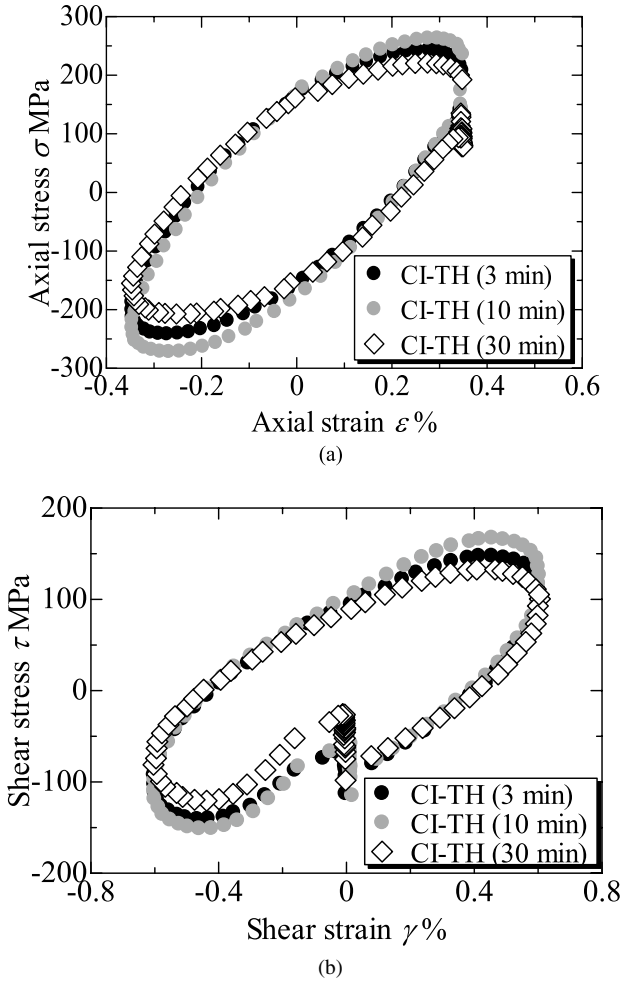

Fig. 9 Hysteresis loops under CI-TH (3 min), CI-TH (10 min) and CI-TH (30 min). **a** Axial stress-axial strain **b** shear stress-shear strain

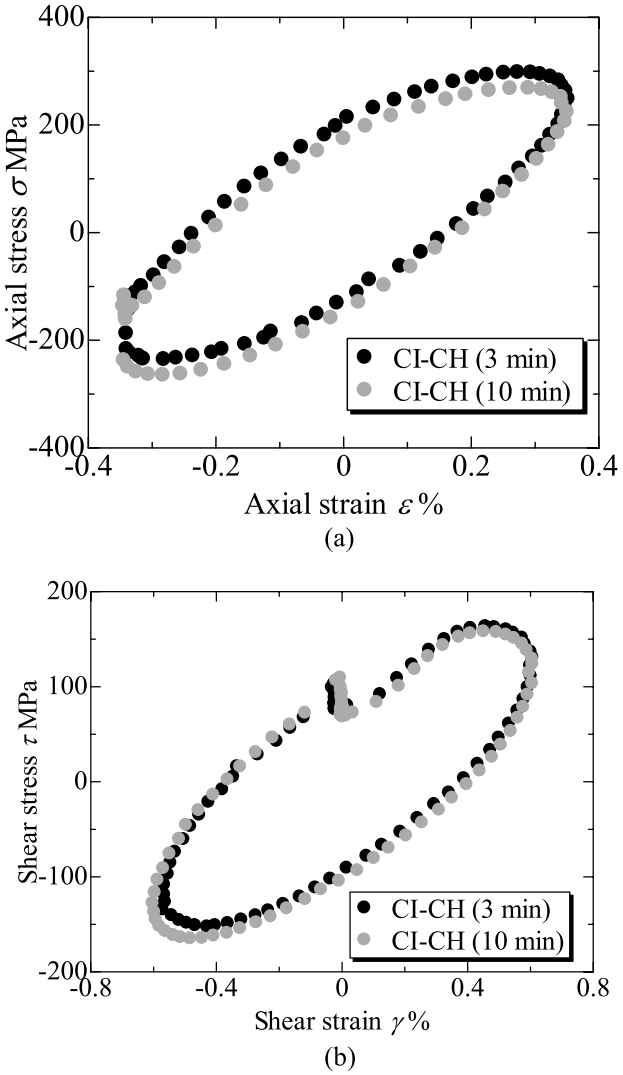

Fig. 10 Hysteresis loops under CI-CH (3 min) and CI-CH (10 min). **a** Axial stress-axial strain **b** shear stress-shear strain

shows the variation of mean axial stress with cycles. Axial stress, particularly the stress range is dominant in the multiaxial failure under compression strain holding. As evidence, mean stress stabilizes at half of failure life. Figure 14 (d) shows the variation of mean torsional stress with cycles; the torsional stress changes linearly under the effect of both the axial strain (with compression holding) and torsional strain. As the conclusion of this section, the following should be noted: stress amplitude and mean stress stabilize just at half of failure life, and in tension strain holding, torsional stress is dominant, while in the compression strain holding, the normal stress range is dominant for multiaxial creep–fatigue failure.

Observation Results of Failed Specimen

This section presents the observation result of the failed specimen after creep–fatigue tests. In the following, the methods for preparing the samples and observation are explained. The central position of the failed specimen was cut to a semi-circular shape and the outer surface was polished with emery paper (#600, #1000, #2000). Then, the texture was etched with picric acid solution, followed by observation of the peripheral zone of main cracks via scanning electron microscopy (SEM). Figure 15 shows the observation results; The left column shows the low magnification image, while the right column shows the high magnification image. First, in the PP-FF test without strain holding, the surface of the specimen and vicinity of the main crack was more uneven than in the other tests, probably due to the high stress generated during the testing. In the PP-SS* test, some creep damage, i.e., the generation of pores on the surface, was observed, but to a lesser extent. In comparison, the specimen surface of PP-SS was relatively smooth, suggesting that the effect of stress was more significant in

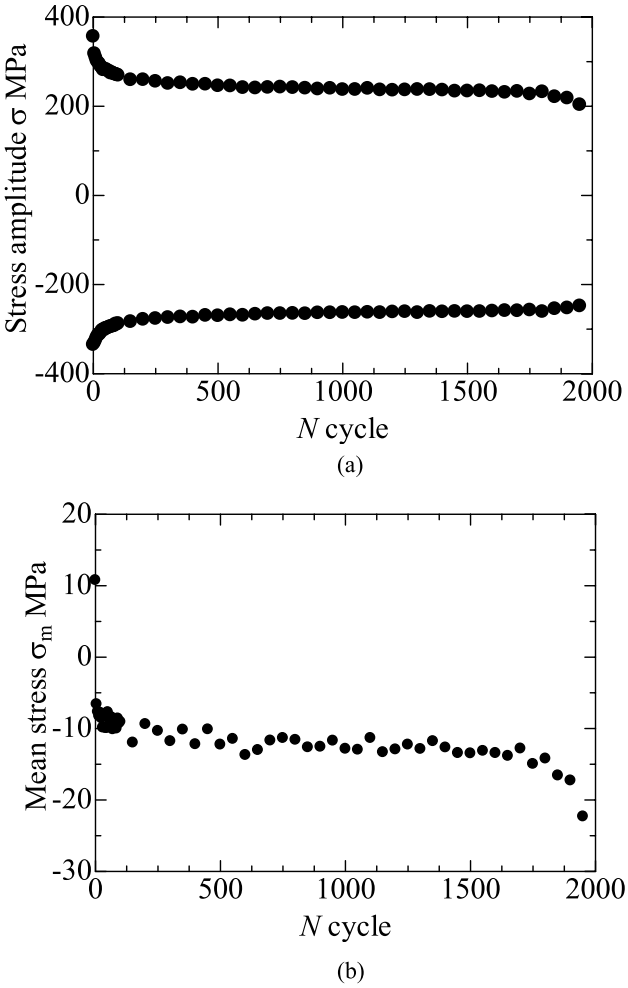

Fig. 11 Stress amplitude and mean stress under PP-TH (3 min). **a** Stress amplitude **b** mean stress

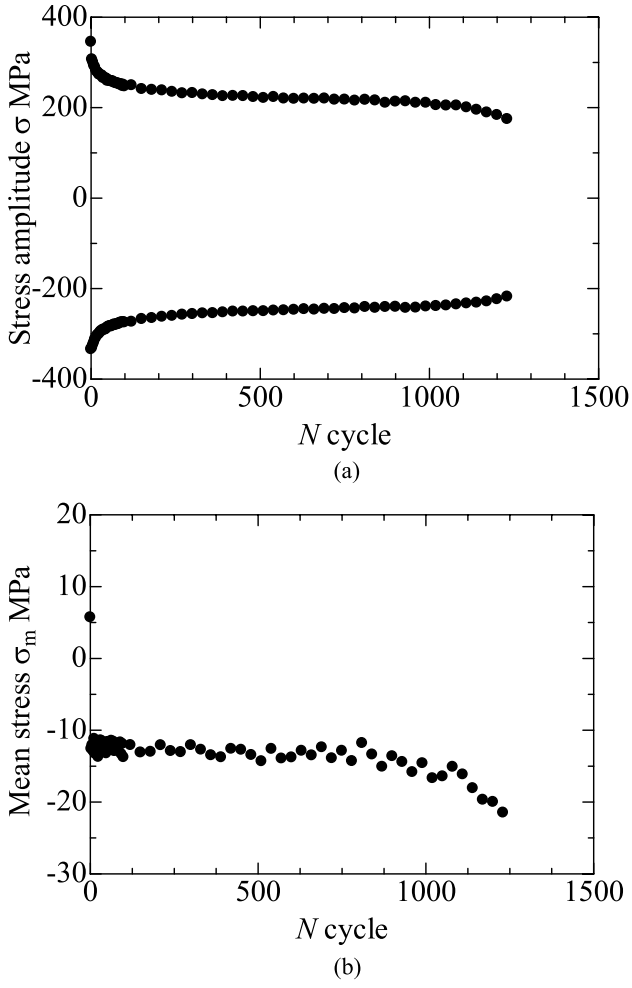

Fig. 12 Stress amplitude and mean stress under PP-TH (10 min). **a** Stress amplitude **b** mean stress

PP-FF. Conversely, the effect of creep was more significant in PP-SS* than in the other tests. In the following, the results for PP-TH loading are presented. The degree of oxidation of the specimens differed depending on the test time, but the appearance of small cracks was similar, and there were no significant irregularities as in the case of PP-FF. In particular, there was no significant difference in the surface appearance of the PP-TH (10 min) and PP-TH (30 min) specimens. However, it appears that the number of small cracks is larger in PP-TH (30 min). Finally, the SEM observation results of the specimen surface of PP-CH are presented. Both PP-CH (3 min) and PP-CH (10 min) showed cracks of similar shape, but the number of cracks was higher in PP-CH (10 min), which justifies life reduction. The fracture morphology and damage sustained in the creep–fatigue test with compression strain holding differed significantly from the fatigue test and the creep–fatigue test with tensile strain holding due to the increase in mean tensile stress. The axial cracks connecting cracks transverse to the loading direction reflect the stress range generated due to compression strain holding along with torsional strain. This study presents only the observation results for proportional loading, and that for non-proportional loading remains a future task.

Evaluation of Strain Energies and Failure Life Correlation

Evaluation of Strain Energies

Figure 16 shows a schematic of how to calculate strain energy density from the hysteresis data. The area between the hysteresis loop on the positive side of stress at 1/2 N_f and the strain axis was calculated (Ellyin and Kujawski 1984). The area inside the hysteresis loop is denoted inelastic strain energy density, while the sum of the inside the hysteresis loop and the area between the hysteresis loop and strain axis is denoted total strain energy density. In the following,

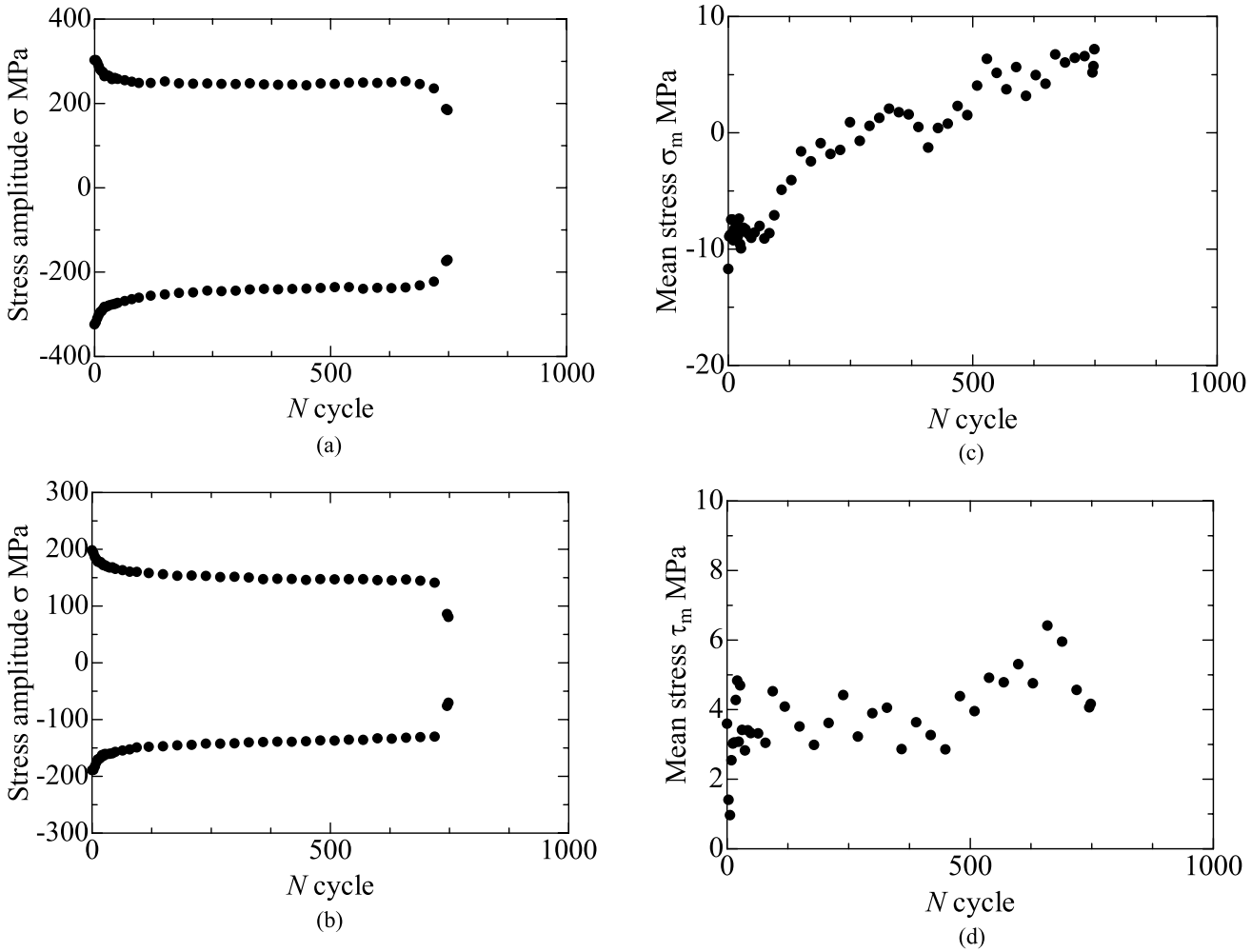

Fig. 13 Stress amplitude and mean stress under CI-TH (3 min). **a** Amplitude of axial stress **b** amplitude of torsional stress **c** mean axial stress **d** mean torsional stress

we explain the calculation method of the strain energy density. The stress value was multiplied by the increment of strain value; The stress was assumed to change step by step, and the divided quadrature method has been adopted. Figure 16 demonstrates the concept for calculating the area. As mentioned later, the effect of the mean stress has been considered. Summation with additional energy was taken by multiplying the mean stress and strain range. Regarding the estimation of strain energy density for evaluation of creep–fatigue lives, Zhu et al. proposed the calculation method of strain energy. They justified that it can include toughness of materials through theoretical consideration (by multiplying the stress and failure strain). In this study, the authors take similar lines; however, this study focuses on estimating experimental energy value, followed by the life correlation of multiaxial creep-fatigue failure.

Figure 17 shows the calculation results of strain energy density from the hysteresis loops of proportional loading conditions. The trends in strain energy densities are similar in the inelastic strain energy density and total strain energy density. In the following, the detail of the energies is explained. The most prolonged failure life corresponds to PP-TH (3 min) with a middle strain energy density. For longer strain holding duration (PP-TH (10 min) and PP-TH (30 min), failure life gets smaller, although strain energy densities are nearly the same as that of PP-TH (3 min); The height between the maximum stress and minimum stress is dominant (indirectly, dependent on the degree of stress relaxation) in the failure regardless of the absence in this consideration. This point will be pursued further in future publication through modeling of hysteresis loops. Regarding the effect of strain rates, in PP-FF, which has the most enormous strain rate, strain energy density has the median value among all conditions, while in PP-SS*, which has the lowest strain rate, strain energy density is the smallest. In strain holding on the compression side, strain energies have

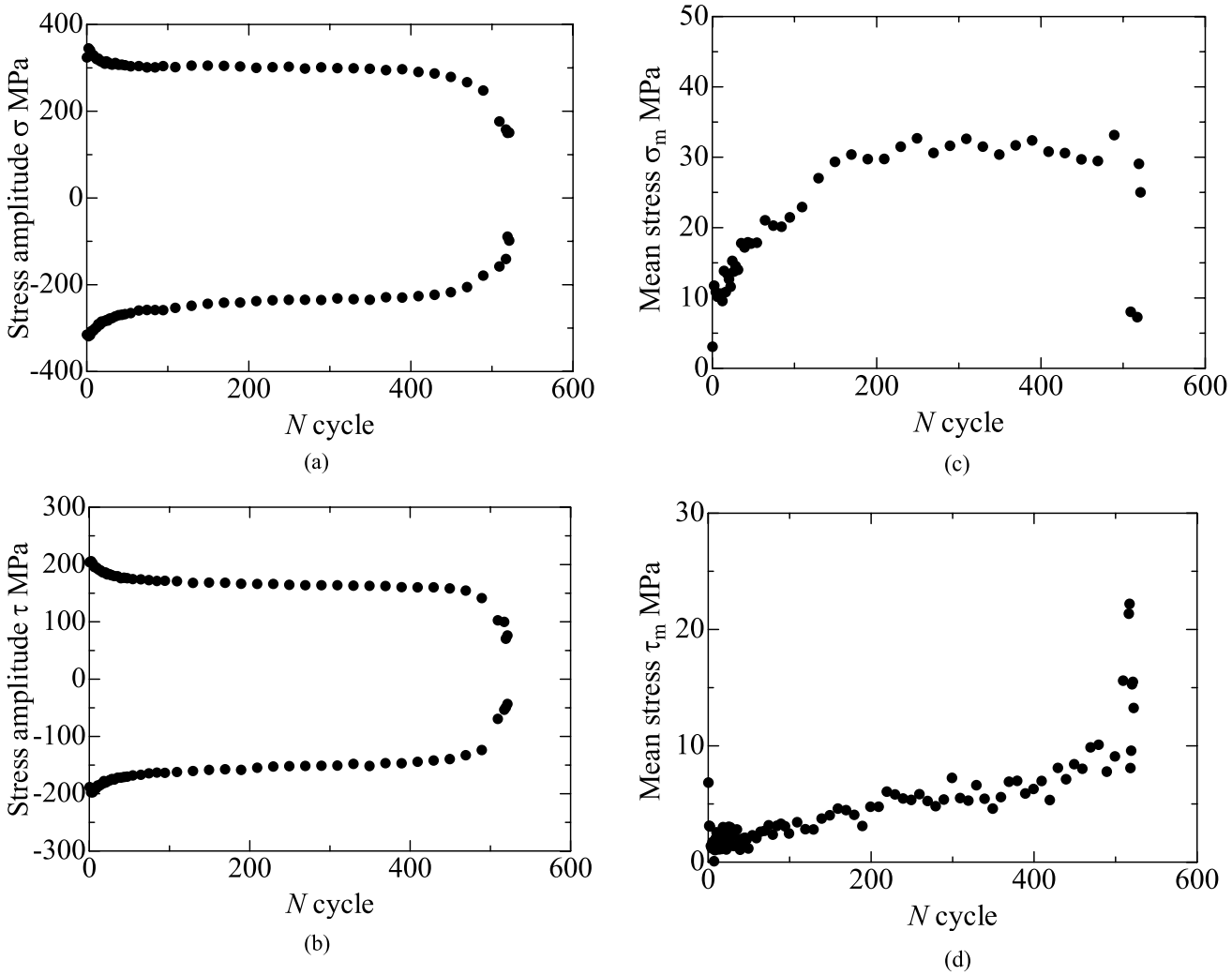

Fig. 14 Stress amplitude and mean stress under CI-CH (3 min). **a** Amplitude of axial stress **b** amplitude of torsional stress **c** mean axial stress **d** mean torsional stress

a high value compared to other loading conditions for almost all conditions. We adopt the inelastic strain energy density because it can distinguish the length of strain holding durations. While in the case of using total strain energy density, energy values do not vary even for short and long strain holding duration. The energy value does change through the balance between elastoplastic deformation and stress variation during strain holding; The adoption of inelastic strain energy density can consider this point.

Figure 17 (b) shows inelastic strain energy density values, which consider the effect of mean stress. How to include the impact of mean stress is schematically demonstrated in Fig. 18 (Wang et al. 2020). Strain holding on the tension side generates compressive mean stress σ_m. Thus, inelastic strain energy density increases by the area between mean stress and strain axis. Energy value becomes the sum of inelastic strain energy W_{in} and ΔW_{in}. Contrary to tension holding, inelastic strain energy density decreases in the case of compressive strain holding due to positive mean stress. The details can be found in Ref. [22].

In Fig. 17 (b), all the data are almost on one straight line, excluding the plot of PP-TH (3 min). The authors' literature study clarified that failure lives are determined between the balance of decrease stress and reduction of strength during stress relaxation accompanying strain holding (Fukuike et al. 2019). Decrease in stress leads to longer failure life, while stress relaxation during strain holding causes the reduction of failure life. It is considered that the maximum stress and the amount of stress relaxation govern failure life. Thus, Fig. 19 investigates and summarizes the relationship between the maximum stress in the hysteresis loops and the amount of stress relaxation.

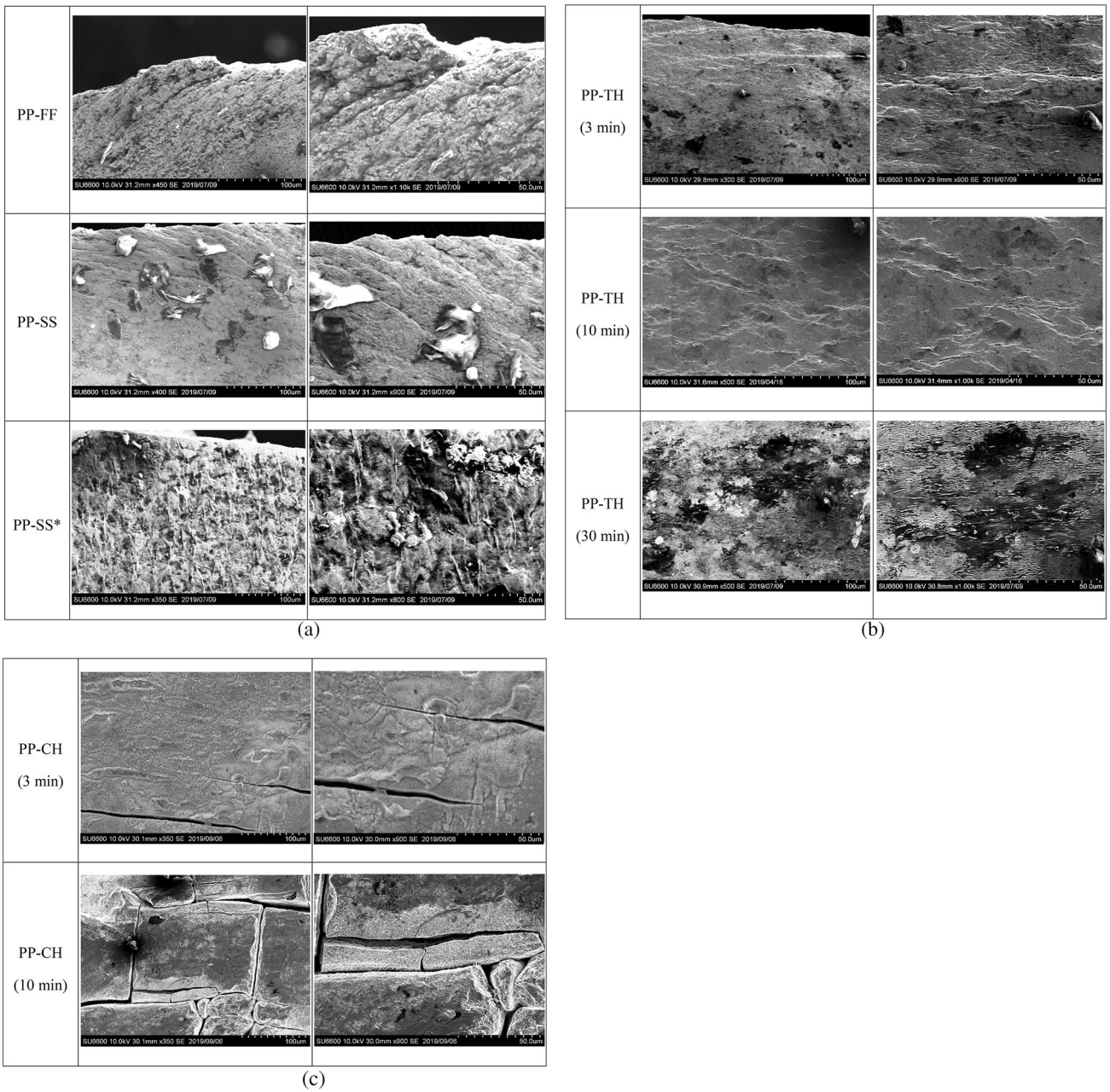

Fig. 15 Observation results of failed specimens via scanning electron microscopy. **a** Push–pull loading **b** PP-TH loading **c** PP-CH loading

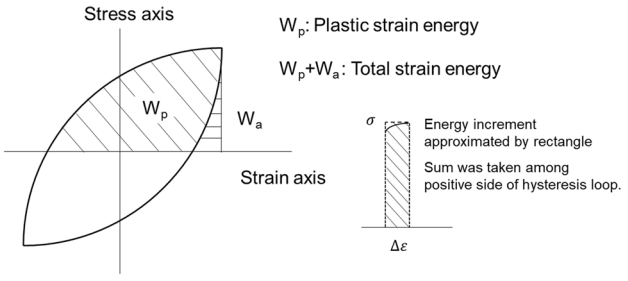

Fig. 16 Schematic of the estimation of strain energy

It is elucidated that a clear correlation between the maximum stress and the amount of stress relaxation exists, and we propose the following energy correction method.

$$\overline{W}_{\text{in}} = W_{\text{in}} \times \frac{\sigma_{\max}}{2\sigma_{\text{min\_holding}}}. \quad (1)$$

$\sigma_{\max}$ is the maximum stress in the hysteresis loops, while $\sigma_{\text{min\_holding}}$ is the minimum stress value during strain holding. The correction factor is $\sigma_{\max}$ divided by $\sigma_{\text{min\_holding}}$; increased maximum stress increases strain energy density. Similarly, the

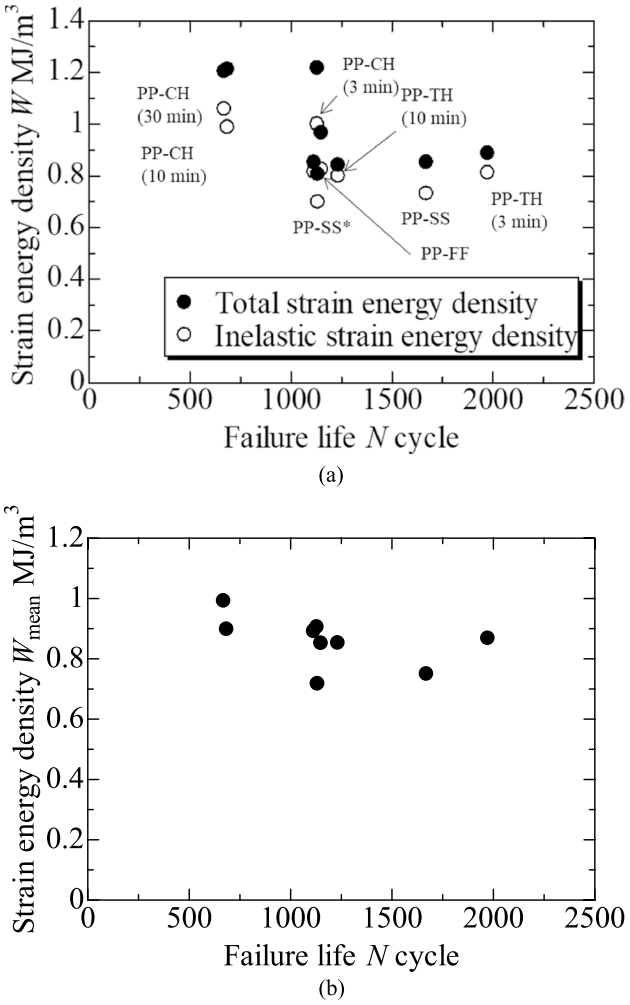

Fig. 17 Strain energy densities calculated from the proportional loading paths. **a** Comparison of inelastic strain energy and total strain energy **b** inelastic strain energy considering the effect of mean stress

higher the amount of stress relaxation, the strain energy density increases. Factor 2 considers the weight of the effect of the maximum stress and stress relaxation. In past studies, the impact of stress relaxation was found to be larger and about twice that of the maximum stress in creep-fatigue loading (Alsmadi et al. 2020; Chen et al. 2020).

The correction factor is set to unity in push–pull loading without strain holding. Strain energy densities were calculated based on Eq. (1) for proportional and non-proportional loading. Note that for compressive strain holding, the maximum stress was set to be that in the tension side, and stress relaxation value was set to be that in the compressive side to consider the effect of stress range on failure lives.

Here, strain energy densities for non-proportional loading were calculated using the following equation [15].

$$\overline{W}_{\text{in\_non-proportinal}} = \overline{W}_a + 2\overline{W}_t. \quad (2)$$

$\overline{W}_a$ is inelastic strain energy density for axial loading, while $\overline{W}_t$ is inelastic strain energy density for torsional loading. Strain energy equals that calculated using 6×6 elements of strain values. It should be noted that correction of strain energies for PP-CH loading was based on the absolute value of minimum stress in the hysteresis loops to consider the difference between the tension holding and compression holding in the non-proportional loading: the formation of cracks in surface oxide in compression loading.

Figure 20 summarizes inelastic strain energy density considering the effect of the mean stress after correcting the maximum and minimum stress. Generally, strain energy density for non-proportional multiaxial loading is three times a value of uniaxial loading (Sharooi et al. 2010; Nagode and Šeruga 2016). Thus, those for multiaxial loading are divided by 3 to correlate with uniaxial loading. Strain energy densities are plotted almost within a factor of 2 bands as shown in Fig. 15.

Failure Life Correlation

This section presents the calculation of the theoretical failure life of Mod. 9Cr-1Mo steel at 823 K under uniaxial proportional loading and non-proportional multiaxial loading. Database for the relationship between strain energy densities and failure life for uniaxial loading is referred from the joint research report with the Japan Atomic Energy Agency (Japan Atomic Energy Agency 2020). The condition is as follows: temperature is 823 K, strain range is 0.69%, the duration of strain holding is 1 h (we select this condition considering the effect of duration needed to be heated up to 823 K). Figure 21 shows the relationship. The horizontal axis is the strain energy density, and the vertical axis is the experimental failure life. The strain energy density is normalized by its maximum value because the stress condition varies depending on the testing machine used for the uniaxial testing. Higher the strain energy density, the shorter the failure life. The strain energy is the driving force of fatigue failure. The polynomial approximation is applied to the curve in Fig. 21 and we obtained approximation formula.

Theoretical failure lives have been obtained from the approximation formula of Fig. 21 and the normalized value of the experimentally obtained strain energy densities shown in Figs. 20, 22 shows the relationship between the experimental and theoretical failure life. Almost all data can be correlated between a factor of 5 bands and a factor of 2 bands using strain energy density. We believe that energy-based methodology has been more effective than the stress-based method. When the data are correlated within a factor of 5 bands, it should be directly helpful for designing

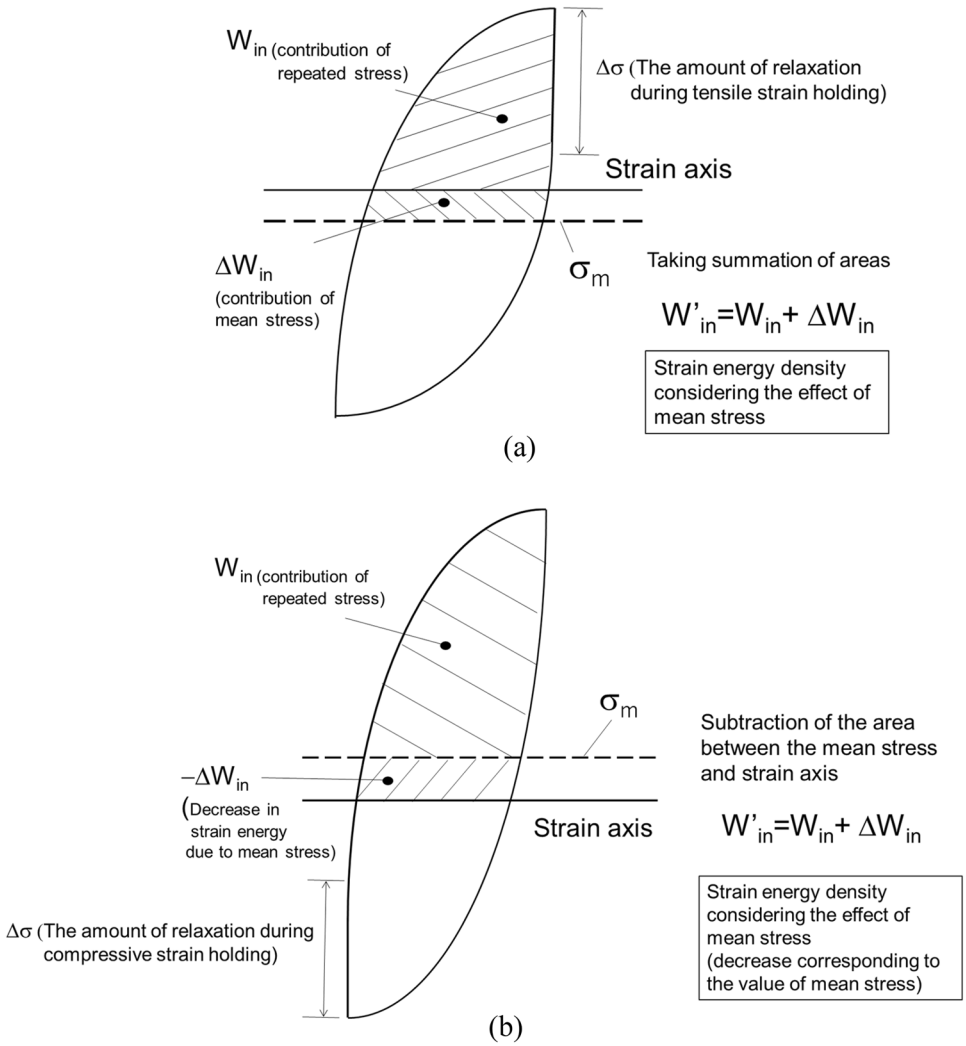

Fig.18 Schematic of the consideration of the effect of mean stress. **a** Strain holding on the tension side **b** strain holding on the compression side

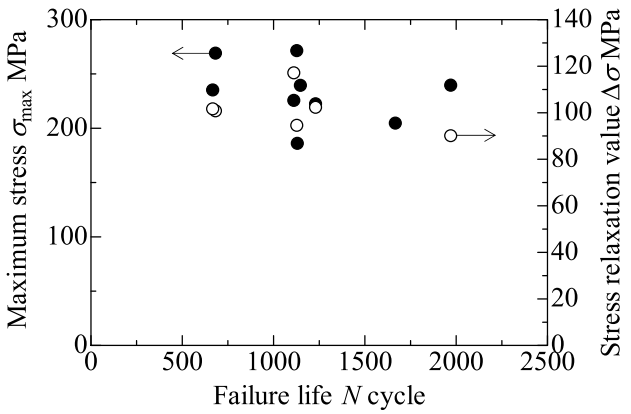

Fig. 19 Relationship between the maximum stress and relaxation stress value

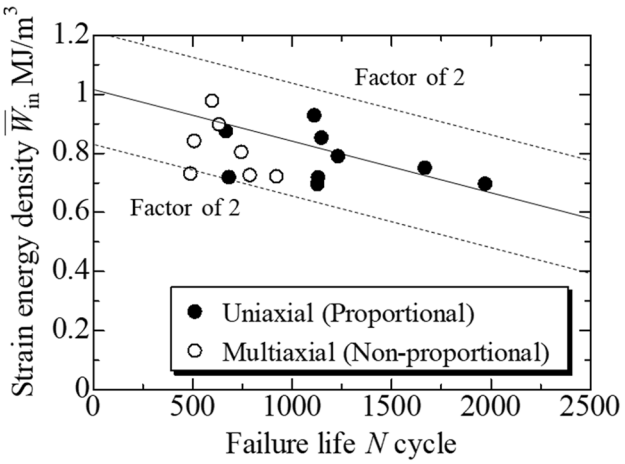

Fig. 20 Normalized value of strain energy density for proportional and non-proportional loading: values of the non-proportional loading are divided by three which is the ratio with proportional loading

components. However, the data for the PP-TH (30 min) have been largely evaluated on the conservative side (on the factor of 10.5 bands), of which reason will be investigated later.

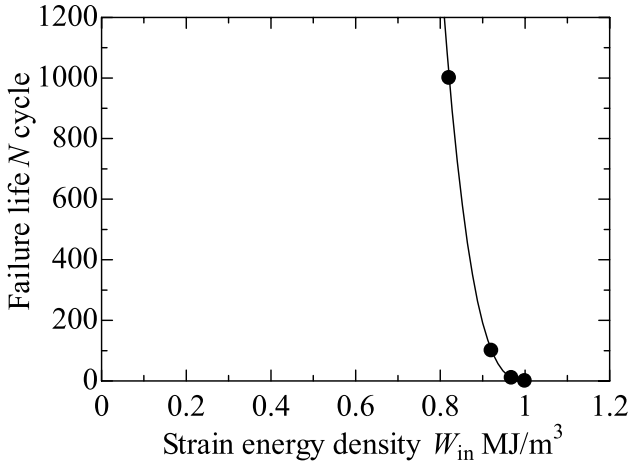

Fig. 21 The relationship between strain energy density and experimental failure life. (based on the report of joint research with the Japan Atomic Energy Agency)

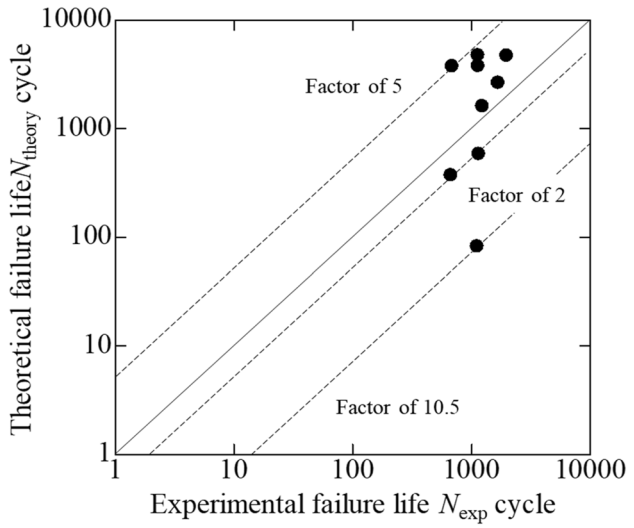

Fig. 22 Results of the life correlation of proportional loading based on the proposed strain energy-based method

Figure 23 summarizes the results for non-proportional multiaxial loading. Almost all data can be correlated between a factor of 5 bands and a factor of 3 bands, regardless of the severity of the loading. The data for CI-SS with the smallest strain rate is evaluated excessively on the conservative side as shown in the circle.

In the following, we investigate the reason for the deviation of the plots on the conservation side by looking into hysteresis loops. For PP-TH (30 min), excessive stress relaxation during strain holding occurs, and the usage of Eq. (1) might lead to the overestimation of inelastic strain energy density. Generally, stress is transferred from the strain-holding region around cracks to the circumference region; Thus, the stress relaxation effect on failure life (damage) gets

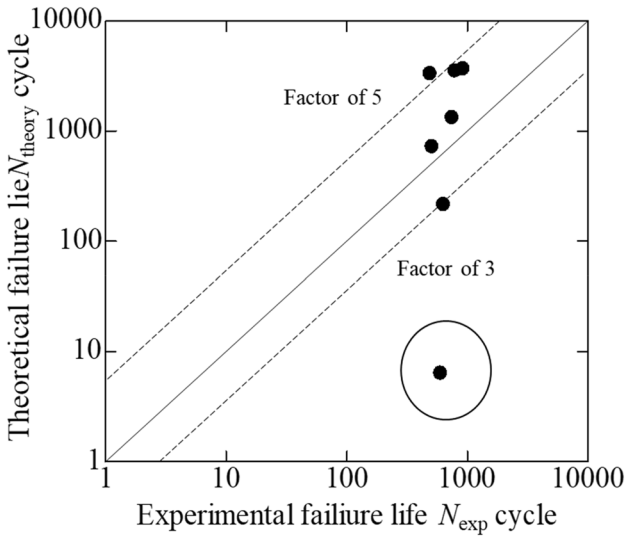

Fig. 23 Results of the life correlation of non-proportional loading based on the proposed strain energy-based method

smaller. We need to consider this effect to achieve higher accuracy. Regarding Fig. 21, in CI-SS of which the strain rate is the smallest, hysteresis data cannot be presented in the limit of pages; however, it should be noted that the inelastic strain ranges in CI-SS increases (from 0.40% to 0.55%) compared to CI-FF, instead of a decrease in the maximum stress. The authors consider the following assumption. If the strain rate is low and the material possesses enough time to extend its plastic region, the inelastic strain range increases. Alternatively, extensive stress relaxation occurs after the passage of a long time, and the failure region inside the material should become narrow. Therefore, in such a case, simply calculating the area inside the hysteresis loop is inadequate. In the creep–fatigue under non-proportional multiaxial loading, it is essential to consider a spatial variation of stress value near and apart cracks and an associated variation of local inelastic strains. We will study this point in the future. The authors believe that the theoretical modeling of inelastic strain energy is essential to consider the intrinsic failure mechanism governing creep-fatigue under non-proportional multiaxial loading at high temperatures. This point should also be investigated soon. We confirm the simple correlation of trends in strain energy densities with the failure mode of specimens. The accumulation of small cracks leading to the nucleation of the main crack dominates failure under tension strain holding. Conversely under the compressive strain holding the axial cracks connects the cracks transverse to the loading direction, which justifies the stress range governs the failure process. Interruption tests have also been conducted, and observation of damages via electron backscattered diffraction will be performed. A detailed study of the failure process will also be reported in successive papers.

Conclusions

1. Non-proportional multiaxial creep-fatigue tests of Mod. 9Cr-1Mo steel were performed. Specificity regarding the strain rate effect and the effect of strain holding was found. At the maximum strain rate, increased maximum stress shortened failure life. In the strain holding of 3 min on the tension side, failure life got larger. This is due to the decrease in stresses on the positive side.
2. Dependence on maximum stress and stress relaxation during strain holding governs failure life during creep–fatigue life. Strain energy densities were calculated based on the area inside hysteresis loops. The correction method of energies based on the maximum stress in the hysteresis loops and minimum stress during the strain holding was proposed.
3. Life correlation was performed using experimentally obtained strain energy densities and the relationship between strain energy density and failure life in uniaxial loading (database). The data were a correlated factor of 5 and of 2 (in the case of non-proportional loading: factor of 3) bands. The possibility of life evaluation under creep–fatigue loading using strain energy density was presented.
4. The data of PH-TH loading with the most prolonged strain holding duration loading and the data with CI-SS loading with the minimum strain rate were evaluated excessively on the conservation side. Importantly, by studying hysteresis loops, it was elucidated to consider the spatial variation of stress value near and apart cracks, and the associated variation of local inelastic strains.

Acknowledgements The authors thank Ms. S. Noguchi, Mr. T. Sakurai at the University of Fukui for conducting the CI test, and Mr. K. Fukuike, M. Okamoto, and Ms. S. Suzuki at Ritsumeikan University for running the PP test. In particular, Mr. K. Fukuike is acknowledged for taking photos of the specimens failed under proportional loading. Dr. F. Ogawa acknowledges the support of The Iron and Steel Institute of Japan through ISIJ Research Promotion Grant. Mr. Fan Liu is acknowledged for checking the quality of English in the manuscript and the contribution for the improvement to the publishable quality.

Funding There is no funding source for this study.

Availability of data and materials The data that support the findings of this study are available from the corresponding author (first author), Fumio Ogawa, upon reasonable request.

Declarations

Conflict of interests All co-authors have seen and agree with the contents of the manuscript and there is no financial interest to report. We certify that the submission is original work and is not under review at any other publication.

References

Alsmadi ZY, Alomari A, Kumar N, Murty KL (2020) Effect of hold time on high temperature creep-fatigue behavior of Fe–25Ni–20Cr (wt.%) austenitic stainless steel (Alloy 709). Mater Sci Eng 771:138591. https://doi.org/10.1016/j.msea.2019.138591

Berto F, Lazzarin P, Gallo P (2014) High-temperature fatigue strength of a copper-cobalt-beryllium alloy. J Strain Anal Eng Des 49:244–256. https://doi.org/10.1177/0309324713511804

Brnic J, Turkarj G, Canadija M, Lanc D, Brnic M (2015) Study of the effects of high temperatures on the engineering properties of steel 42CrMo4. High Temp Mater Proc 34:27–34. https://doi.org/10.1515/htmp-2014-0011

Chen S, Wei D, Wang J, Wang Y, Jiang X (2020) A new fatigue life prediction model considering the creep-fatigue interaction effect based on the Walker total strain equation. Chin J Aeronaut 33:2382–2394. https://doi.org/10.1016/j.cja.2020.06.001

Doong SH, Socie DF (1991) Constitutive modeling of metals under nonproportional cyclic loading. J Eng Mater Technol 113:23–30. https://doi.org/10.1115/1.2903379

Doong SH, Socie DF, Robertson IM (1990) Dislocation substructures and nonproportional hardening. J Eng Mater Tech-Nol 112:456–464. https://doi.org/10.1115/1.2903357

Ellyin F, Kujawski D (1984) Plastic strain energy in fatigue failure. J Press Vessel Technol 106:342–347. https://doi.org/10.1115/1.3264362

Evaluation of creep-fatigue properties of Mod. 9Cr-1Mo steel and elucidation of failure mechanism, Report of joint research of Japan Atomic Energy Agency and Ritsumeikan University, University of Fukui and Tohoku University (2020)

Fan Y-N, Shi HJ, Tokuda K (2015) A generalized hysteresis energy method for fatigue and creep-fatigue life prediction of 316L(N). Mater Sci Eng A 625:205–212. https://doi.org/10.1016/j.msea.2014.11.097

Fleischer RL (1985) High-temperature, high-strength materials-An overview. JOM 37:16–20. https://doi.org/10.1007/BF03259961

Fukuike K, Ogawa F, Hiyoshi N, Itoh T (2019) Evaluation of creep-fatigue properties for Mod.9Cr-1Mo steel under proportional and non-Proportional loading, Proceedings of 10th Japan-China Bilateral Symposium on High Temperature Strength of Materials 192–196

Holdsworth S (2019) Creep-ductility of high temperature steels: A review. Metals 9:342. https://doi.org/10.3390/met9030342

Huffman PJ (2016) A strain energy based damage model for fatigue crack initiation and growth. Int J Fatigue 88:197–204. https://doi.org/10.1016/j.ijfatigue.2016.03.032

Itoh T, Sakane M, Morishita T (2015) Evaluation and visualization of multiaxial stress and stress states under non-proportional loading. Frattura Integr Strutt 9:289–301. https://doi.org/10.3221/IGF-ESIS.33.33

Kasamuta Y, Ogawa F, Itoh T, Tanigawa H (2019) Evaluation of multiaxial creep-fatigue strength for high Chromium steel under non-proportional loading. Matec Web of Conferences 300:07002. https://doi.org/10.1051/matecconf/201930007002

Mroziński S, Lis Z, Egner H (2021) Energy dissipated in fatigue and creep conditions. Materials 14:4724. https://doi.org/10.3390/ma14164724

Nagode M, Šeruga D (2016) Fatigue life prediction using multiaxial energy calculations with the mean stress effect to predict failure of linear and nonlinear elastic solids. Results Phys 6:352–364. https://doi.org/10.1016/j.rinp.2016.06.007

Nakayama Y, Ogawa F, Hiyoshi N, Hashidate R, Wakai T, Itoh T (2021) Evaluation of multiaxial low cycle creep-fatigue life for Mod. 9Cr-1Mo steel under non-proportional loading. ISIJ

International Accepted. https://doi.org/10.2355/isijinternational.ISIJINT-2020-780

Ozaltun H, Shen MHH, George T, Cross C (2011) An energy based fatigue life prediction framework for in-service structural components. Exp Mech 501:707–718. https://doi.org/10.1007/s11340-010-9365-z

Payten WM, Dean DW, Snowden KU (2010) A strain energy density method for the prediction of creep-fatigue damage in high temperature components. Mater Sci Eng A 527:1920–1925. https://doi.org/10.1016/j.msea.2009.11.028

Plumbridge WJ, Dean MS, Miller DA (1982) The importance of failure mode in fatigue-creep interactions. Fatigue Fract Eng Mater Struct 5:101–114. https://doi.org/10.1111/j.1460-2695.1982.tb01228.x

Scott-Emuakpor O, George T, Cross C, Shen MHH (2010) Multi-axial fatigue life prediction via a strain-energy method. AIAA J 48:63–72. https://doi.org/10.2514/1.39296

Sharooi S, Metselaar IH, Huda Z (2010) Evaluating a strain energy fatigue method using cyclic plasticity models. Fatigue Fract Eng Mater Struct 33:530–537. https://doi.org/10.1111/j.1460-2695.2010.01463.x

Takahashi Y, Yaguchi M (2005) Modification of ductility exhaustion-type creep-fatigue Life Prediction method based on re-definition of creep damage and application to high-chromium steels. J Soc Mater Sci Jpn 54:168–173. https://doi.org/10.2472/jsms.54.168

Wang CH, Brown MW (1993) A path-independent parameter for fatigue under proportional and non-proportional loading. Fatigue Fract Eng Mater Struct 16:1285–1297. https://doi.org/10.1111/j.1460-2695.1993.tb00739.x

Wang RZ, Zhang X-C, Tu S-T, Zhu S-P, Zhang C-C (2016) A modified strain energy density exhaustion model for creep-fatigue life prediction. Int J Fatigue 90:12–22. https://doi.org/10.1016/j.ijfatigue.2016.03.005

Wang Q, Xu Z, Wang X (2020) An efficient fatigue and creep-fatigue life prediction method by using the hysteresis energy density rate concept. Fatigue Fract Eng Mater Struct 43:1529–1540. https://doi.org/10.1111/ffe.13230

Zhu SP, Huang HZ, He L-P, Liu Y, Wang Z (2012) A generalized energy-based fatigue-creep damage parameter for life prediction of turbine disk alloys. Eng Fract Mech 90:89–100. https://doi.org/10.1016/j.engfracmech.2012.04.021